

We are IntechOpen, the world's leading publisher of Open Access books Built by scientists, for scientists

6,900

Open access books available

186,000

International authors and editors

200M

Downloads

Our authors are among the

154

Countries delivered to

TOP 1%

most cited scientists

12.2%

Contributors from top 500 universities



WEB OF SCIENCE™

Selection of our books indexed in the Book Citation Index
in Web of Science™ Core Collection (BKCI)

Interested in publishing with us?
Contact book.department@intechopen.com

Numbers displayed above are based on latest data collected.
For more information visit www.intechopen.com



3D Seismic Velocity Structure Around Plate Boundaries and Active Fault Zones

Mohamed K. Salah

Additional information is available at the end of the chapter

<http://dx.doi.org/10.5772/65512>

Abstract

Active continental margins, including most of those bordering continents facing the Pacific Ocean, have many earthquakes. These continental margins mark major plate boundaries and are usually flanked by high mountains and deep trenches, departing from the main elevations of continents and ocean basins, and they also contain active volcanoes and, sometimes, active fault zones. Thus, most earthquakes occur predominantly at deep-sea trenches, mid-ocean spreading ridges, and active mountain belts on continents. These earthquakes generate seismic waves; strong vibrations that propagate away from the earthquake focus at different speeds, due to the release of stored stress. Along their travel path from earthquake hypocenters to the recording stations, the seismic waves can image the internal Earth structure through the application of seismic tomography techniques. In the last few decades, there have been many advances in the theory and application of the seismic tomography methods to image the 3D structure of the Earth's internal layers, especially along major plate boundaries. Applications of these new techniques to arrival time data enabled the detailed imaging of active fault zones, location of magma chambers beneath active volcanoes, and the forecasting of future major earthquakes in seismotectonically active regions all over the world.

Keywords: 3D seismic structure, seismic tomography, V_p/V_s ratio, plate boundaries, crustal structure

1. Introduction

Benefiting from the recent, large computer powers and the increasing quality and quantity of the available seismological data, seismologists developed a new research field of seismology termed "*seismic tomography*." Seismic tomography is like taking a CT scan of the Earth, using

seismic waves to make images of the Earth's interior. The obtained images are used to understand not only the composition of the Earth's interior, but also to explain geologic mysteries such as the formation of mountain chains and the extensive volcanism in certain regions of the Earth. Through these images, scientists can deduce what types of rocks make up the deep Earth's layers and what are the processes operating inside it from earthquake recordings on the surface. Previous studies indicate that rupture nucleation and earthquake generating processes are closely associated with heterogeneities of crustal and upper mantle materials and the inelastic processes in the fault zones, including the migration of fluids [1]. Seismic tomography techniques were used extensively to image the deep structure of subduction zones, which are considered as key elements in plate tectonics. They were also used to image hot springs, and the nucleation zones of large destructive earthquakes as well as the growth of earthquake rupture along active faults [2–4].

2. Tectonic plate boundaries and active fault zones

The tendency of earthquakes to occur in relatively narrow belts was one of the key lines of evidence leading in the 1960s to the theory of plate tectonics [5]. The surface of the Earth consists of a number of tectonic plates (**Figure 1**), with each plate consisting of the crust and the more rigid part of the upper mantle, which collectively are called the lithosphere. The latter comprises all the world's earthquakes, and it is underlain by a weaker zone termed the asthenosphere, with the lithosphere-asthenosphere boundary controlled by temperature. Although the asthenosphere is solid, it yields by slow creep, allowing solid-state flow that compensates for the motion of the overriding lithospheric plates. The lithosphere may be more than 100 km thick beneath older continental regions, but it is only a few kilometers thick beneath mid-ocean ridges, where it first forms. Lithospheric plates are in continuous motion with respect to one another, and the disruption produced at the boundaries between the plates results in earthquakes (**Figure 2**).

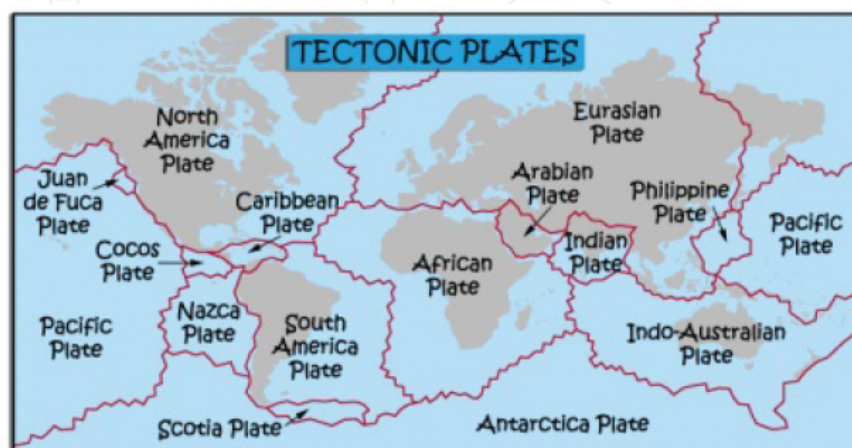


Figure 1. The global pattern of major and minor plates with their boundaries marked in red.

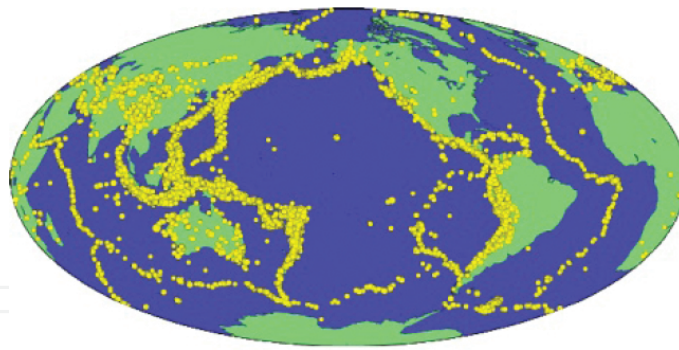


Figure 2. The global distribution of earthquakes along the major plate boundaries.

Mid-ocean spreading ridges are formed by the upwelling of hot magma that cools and solidifies as lithospheric plates move away from the ridge crest, and newly formed oceanic crust is carried down the flanks of the ridge. Earthquakes on spreading ridges are limited to the ridge crest, where a new crust is being formed. The crust is too hot, thus only a thin, near-surface zone is brittle enough to generate earthquakes, which tend to be relatively small and occur at shallow depths. *Deep-sea trenches* form where lithosphere converges, forcing one slab beneath the other. This convergent boundary, called a subduction zone, is defined by a zone of earthquakes (*Wadati-Benioff zone*) that marks where lithosphere extends into the mantle to depths up to 700 km. Earthquakes also occur along zones where the slabs slide past one another; these zones are called *transform faults*. The global distribution of earthquakes defines a mosaic of lithospheric plates up to 100 km thick that are moving with respect to one another. Most of the plate boundaries are defined by earthquake epicenters (**Figures 1 and 2**). Crustal faults, on the other hand, usually have a fault core and surrounding regions of brittle damage, forming a low-velocity zone in the immediate vicinity of the main slip interface [6].

3. Seismic tomography: the imaging technique

In local seismic tomography, body-wave arrival times are used to estimate the *P*- and *S*-wave velocities from which we deduce variations in lithology and physical properties of the rocks below the surface [7]. According to many researchers [8], velocity usually increases with depth; however, in some regions the reverse has been recognized [9]. A brief review of how rock properties relate to seismic velocity and attenuation can be found in Sanders et al. [10], Wu and Lees [11], and Lees and Wu [12]. Among the many factors that affect seismic velocity, the sediment thickness, fractures, and fluid saturation have a great effect on the imaged velocity structure especially at shallow layers. The product of V_p and V_s can be used to identify variations in porosity for shallow crustal rocks but the ratio of V_p and V_s (or Poisson's ratio) is commonly used to delineate lithology [13, 14]. The V_p/V_s ratio is directly related to Poisson's ratio (σ) by the relationship: $(V_p/V_s)^2 = (1 - \sigma)/(1/2 - \sigma)$; and is a useful indicator of lithology and pore fluid pressure. On average, this ratio is equal to 3 corresponding to a σ value of 0.25 for the Earth's crust and upper mantle [15]. Any deviation from this value indicates a change in the physical properties of the constituting rocks.

The seismic tomography method used to image the 3D seismic velocity structure around plate boundaries and active fault zones in the following sections is that of Zhao et al. [16–18]. This method is suitable for a general velocity structure which may include several seismic velocity interfaces and allows for 3D velocity variations in the model. The seismic interfaces represent known geological discontinuities such as the Conrad and Moho or any subducting slab boundary. A 3D grid net, with the proper spacing, is set up in the model to express the 3D velocity structure. Velocity perturbations at the grid nodes are taken as unknown parameters with respect to the initial model. At any other point in the model, the velocity perturbations are calculated by linear interpolation at the eight grid nodes surrounding that point. To calculate travel times and ray paths in an accurate and an efficient way, a 3D ray-tracing algorithm [16] is employed that iteratively uses the pseudo-bending technique [19] in between the discontinuities and Snell's law at interfaces:

$$\frac{\sin \theta_1}{V_1} = \frac{\sin \theta_2}{V_2} \quad (1)$$

where θ_1 and θ_2 are the incident and refraction angles, respectively, and V_1 and V_2 are the respective seismic velocities of two successive layers. Station elevations are taken into account in the ray tracing scheme.

All tomographic problems can be represented by an observation equation relating the data to the medium and source parameters:

$$d = Gm + e \quad (2)$$

where d , m , and e are the data vectors, unknown model parameters, and errors, respectively. G is the coefficient matrix with its elements consisting of travel time derivatives with respect to hypocentral and velocity parameters [1]. For more details about the method, refer to Zhao et al. [16–18].

The optimum grid spacing in the horizontal and vertical directions is usually adopted for a specific study; depending on the available data and the station density. Velocities at grid points are considered to be unknown parameters except those at the outermost grid, which are just used to interpolate velocities outside of the modeling space. According to Zhao et al. [16], the velocity at any point in the m th layer is calculated by using a linear interpolation function:

$$Vm(\varphi, \lambda, h) = \sum_{i=1}^2 \sum_{j=1}^2 \sum_{k=1}^2 Vm(\phi_i, \lambda_j, h_k) \left[\left(1 - \left| \frac{\phi - \phi_i}{\phi_2 - \phi_1} \right| \right) \left(1 - \left| \frac{\lambda - \lambda_j}{\lambda_2 - \lambda_1} \right| \right) \left(1 - \left| \frac{h - h_k}{h_2 - h_1} \right| \right) \right] \quad (3)$$

where ϕ is latitude, λ is longitude, and h is the depth from the Earth's surface; ϕ_i , λ_j , and h_k represent the coordinates for the eight grid nodes surrounding the point (ϕ, λ, h) . $Vm(\phi_i, \lambda_j, h_k)$ is the velocity at the grid net set for the m th layer at a specific location.

After determining the P - and S -wave velocity models, the V_p/V_s ratio can then be calculated in the modeling space. This ratio (or the Poisson's ratio) is a good indicator for the petrophysical properties of crustal rocks and can provide better constraints on the crustal composition and interstitial fluids than either P - or S -wave velocity alone [20–25]. So far, the V_p/V_s ratio has proved to be very significant in the understanding of the seismogenic behavior of the crust, and the role of crustal fluids in the nucleation and growth of earthquake rupture [2, 23, 26–29]. In the following sections, we present the results of the 3D crustal and upper mantle seismic velocity structure at selected areas located near active faults and major plate boundaries. These velocity models are obtained through the application of the seismic tomography technique on available data sets from these regions.

4. Crustal velocity and V_p/V_s structures along the central section of the NAFZ

4.1. Seismotectonic setting

Central Turkey is characterized by coherent plate motion attributed to escape tectonics, involving the westward displacement and counterclockwise rotation of the Anatolian block [30, 31]. This westward extrusion is induced by the northerly directed subduction of the African plate beneath Anatolia to the south of Cyprus [32]. While it is rotating anticlockwise, the Anatolian region is also under approximately N-S and NNE-SSW shortening, related to collision processes between the Anatolian and African plates along the Cyprean arc [33–39]. The Anatolian plate is decoupled from Eurasia along the right-lateral, strike-slip North Anatolian Fault Zone (NAFZ). The existence of the NAFZ and the East Anatolian Fault Zone (EAFZ), and the induced westward escape of the Anatolian block mark the formation of four distinct neotectonic provinces: (1) East Anatolian Contractional Province, (2) North Anatolian Province, (3) Central Anatolia, and (4) West Anatolian Extensional Province [35] (**Figure 3**). The NAFZ is one of the best-known strike-slip faults in the world because of its noticeable seismic activity, induced high stress accumulation, extremely well-developed surface expression, and importance for the tectonics of the eastern Mediterranean region [35, 40–42]. To the east, the NAFZ forms a typical triple-junction and joins with the sinistral EAFZ at Karliova (**Figure 3**). The NAFZ is approximately 1500 km-long, broad arc-shaped, dextral strike-slip fault system that extends from eastern Turkey in the east to Greece in the west [43]. Being subparallel to the coast of the Black Sea, the NAFZ forms the part of the boundary between the Eurasian Plate to the north and the Anatolian Plate to the south (**Figure 3**). Several 2nd order faults that splay from it into the Anatolian Plate also characterize the NAFZ. Central Anatolia hosts also widely distributed volcanics such as the Mio-Pliocene ignimbrites [44] and stratovolcanoes [45].

The analysis of geological data suggests slow rates of motion on the NAFZ varying slightly from about 5–10 mm/yr [46] to 17 ± 2 mm/yr [47], whereas plate motion and seismological data suggest higher rates of 30–40 mm/yr [48]. This discrepancy arises from the exaggerated slip rate obtained by treating the intense seismicity on the NAFZ during 1939–1967 as typical of

all times. However, recent GPS data indicate intermediate present-day rates of about 15–25 mm/yr [30, 39, 49]. The extrapolation of recent rates to early Pliocene yields a total displacement of 75–125 km, which is in close agreement with the estimates of 85 ± 5 km by many researchers [47, 50, 51]. Owing to its current geotectonic setting, central Anatolia is a region where discrete pieces of continental lithosphere have deformed internally and produced a large bulk strain that has resulted in the generation of new structures or reactivation of old structures. Thus, during the past 60 years, the NAFZ has produced strong earthquakes along different sections in a manner that is typical of long faults. Beginning with the 1939 Erzincan earthquake ($M \sim 7.9$ – 8.0), which produced about 350 km of ground rupture, the NAFZ ruptured by nine moderate to large earthquakes ($M \leq 6.7$), and formed more than 1000 km surface rupture along its surface trace [52].

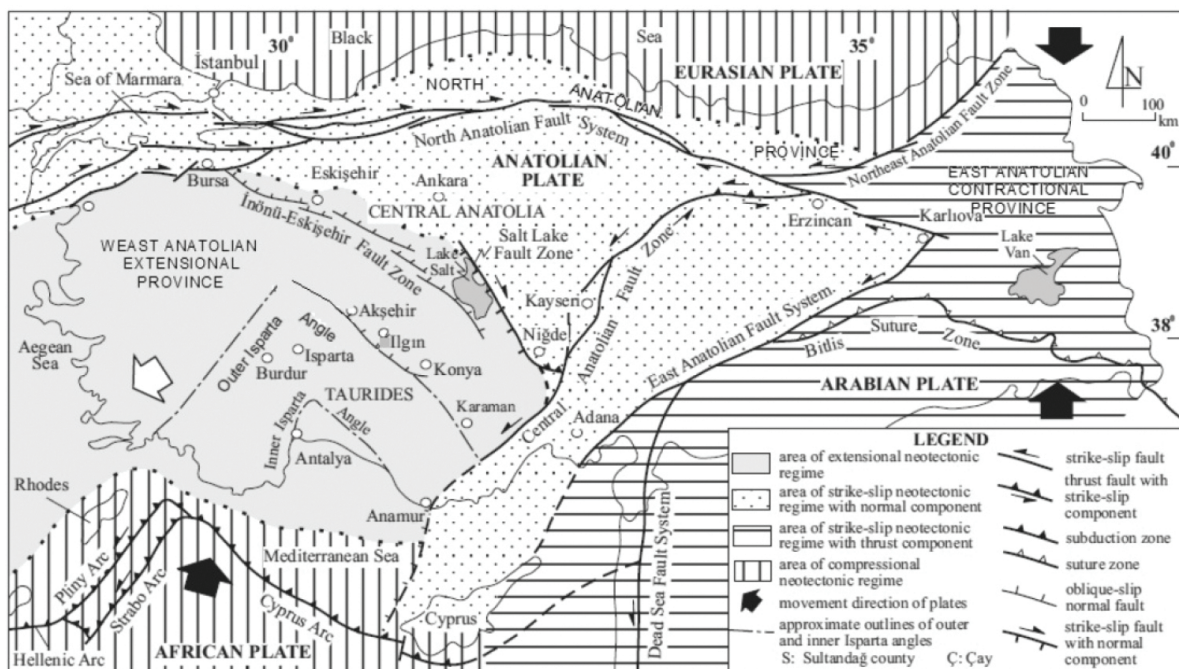


Figure 3. A simplified tectonic map of Turkey showing major neotectonic structures and neotectonic provinces (modified from Koçyiğit and Özacar [53]).

4.2. Data

In this study, we selected a total number of 6549 events that occurred between latitudes 37.5 – 42°N and longitudes 32 – 37°E in the period between 2007 and 2010 (**Figure 4**). These events are recorded by 35 seismic stations belonging to different networks in Turkey (**Figure 4**). The crustal model of Herrin [54] and the HYPO71 source code [55] are used for the routine determination of the hypocentral parameters. The selected events in central Anatolia generated 26,700 and 24,950 P - and S -wave arrivals, respectively [29]. The majority of the earthquakes are located in the central and southeastern parts of the study area with prominent concentration along the active NAFZ and the EAFZ. The approximately equal number of both P - and S -wave arrivals implies that the ray path coverage of the two data sets is similar (**Figure 5**).

The accuracy of arrival times is estimated to be lesser than 0.10 s for *P*-wave data and somewhat larger (<0.15 s) for *S*-wave data.

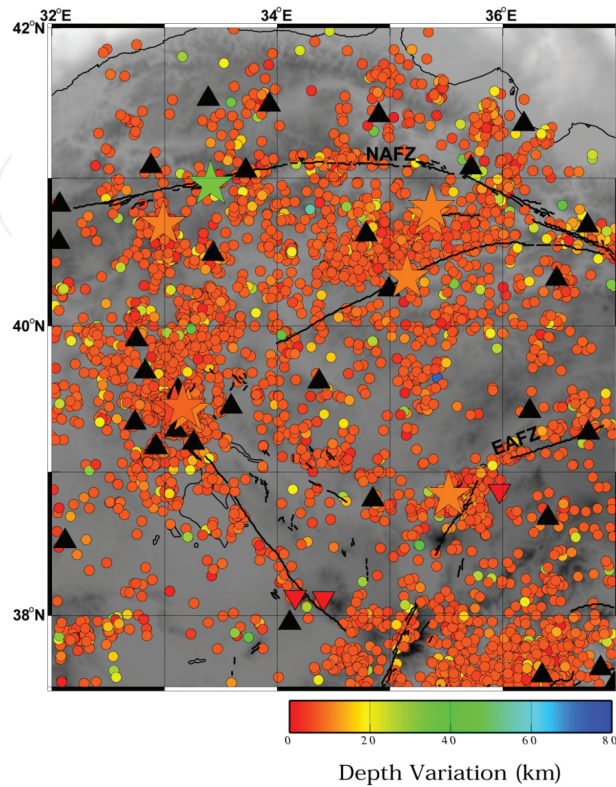


Figure 4. Epicentral distribution of the 6549 earthquakes used in this study shown as circles, which vary in color according to the focal depth (scale is at the bottom). Large stars denote large crustal earthquakes collected from the NEIC catalogs. The black triangles show the 35 seismic stations in central Anatolia. Black lines denote active fault segments of the NAFZ and EAFZ [56]. Inverted red triangles denote the Cenozoic volcanoes.

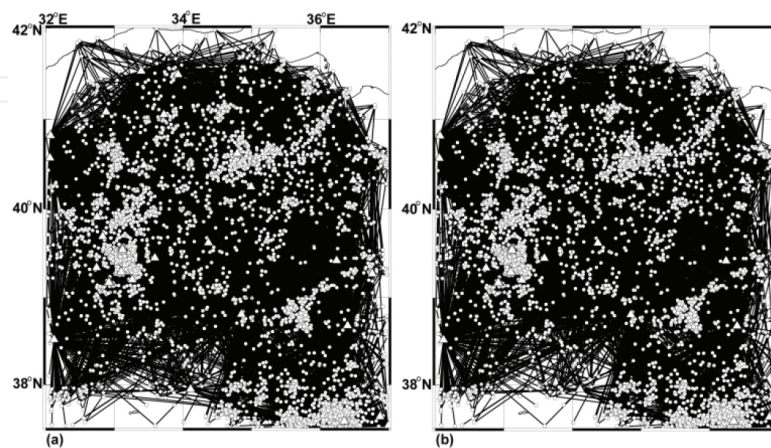


Figure 5. Horizontal ray path coverage of *P*-wave (a) and *S*-wave (b) data sets in plan views. Every path between an event and a recording station is drawn as one straight line. Small open circles and triangles denote events and recording stations, respectively.

Convergence zones are generally characterized by a thick crust [31, 57], which is the case beneath Anatolia especially beneath eastern sector with a progressive decrease in the crustal thickness in the westward direction [58]. We adopted initial P -wave velocities of 5.5, 6.0, and 6.5 km/s at depths above 3, 16, and 33 km, respectively, beneath central Anatolia (refer to Ref. [29] for more details). An initial S -wave velocity model is calculated by using a V_p/V_s ratio of 1.74 deduced from a Wadati diagram (Figure 6) constructed from the present data set.

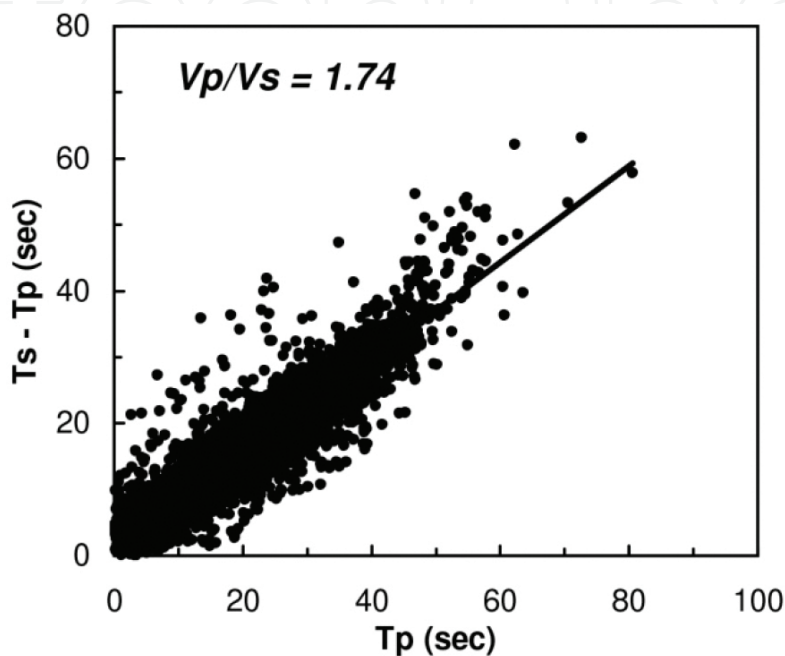


Figure 6. A cumulative Wadati diagram constructed from the arrival time data of the present data set. The resulting V_p/V_s ratio of 1.74 is used to derive the initial S -wave velocity model from the adopted P -wave velocity model (see text for details).

We also collected the list of moderate/large earthquakes (M_b or $M_w \geq 5.0$), which occurred in the study area since 1977 from the catalogs of the National Earthquake Information Center (NEIC), U. S. Geological Survey (Figure 4), to examine the relation between the source areas of these events and the seismic velocity and V_p/V_s anomalies obtained in this study. It is clear that all these nine events are mainly induced by movements along the NAFZ and the EAFZ.

4.3. Results

Applying the tomographic method described previously to the central Anatolia data set (Figure 4), we found that the sum of squared travel-time residuals is reduced by more than 50% of its initial value after three iterations [29]. Inversion results of V_p , V_s , and V_p/V_s distributions at four depth layers are shown, respectively, in Figures 7–9. The velocity images show the velocity perturbations in percentage from the initial velocity model at each depth.

Significant lateral and vertical variations of up to $\pm 8\%$ of velocity (V_p and V_s) and V_p/V_s ratio are revealed in the study area. Lower-than-average velocity anomalies are revealed at most

depth slices especially at a depth of 25 km (**Figures 7 and 8**). The magnitude of the low-velocity anomalies is larger near the NAFZ, EAFZ, and the active volcanoes. In addition, most of the microseismic activity is concentrated along the NAFZ and EAFZ in addition to some heterogeneous zones having low-velocity anomalies. At some depth slices (12 and 40 km), small zones that exhibit high-velocity anomalies are clearly visible, implying the possible presence of strong asperities which are capable of resisting accumulated strain. Thus, the seismic activity at these portions is sparse. The V_p/V_s ratio shows high structural heterogeneity at the different crustal and uppermost mantle layers (**Figure 9**), and is generally higher-than-average at all depth layers, which implies a general low S -wave velocity structure compared to the P -wave velocity. Prominent high V_p/V_s anomalies are evident beneath the active volcanoes and the fault segments. These areas may represent the conduits for the vertically ascending hot fluids from the uppermost mantle beneath central Anatolia. All the moderate/large earthquakes are closely related to the active fault zones, which are characterized generally by the low-velocity/high V_p/V_s ratio (**Figures 7–9**). Microseismic activity, on the other hand, is intense in the central western part of the study area, which is characterized by highly heterogeneous velocity and V_p/V_s structures. The implications of these velocity and V_p/V_s anomalies and their relation to other geophysical investigations beneath central Anatolia are briefly discussed in the following paragraphs.

4.4. Discussion

The obtained velocity and V_p/V_s models beneath central Anatolia show generally low-velocity/high V_p/V_s anomalies, which are consistent with many previous observations and arise mainly from the extensive faulting and the presence of sedimentary basins in the study area [59]. Earlier results of Gürbüz and Evans [60] of the P -wave velocity in the upper crust beneath the Tuzgölü basin, central Turkey, show low P -wave velocities starting from about 2.1 km/s at the surface and gradually increasing to 4.0–4.2 km/s at depths of 5–8 km and ending with a velocity of 6.15 km/s at a depth of 12 km. These near-surface low-velocity zones are interpreted to be caused by evaporites and sedimentary layers. Hearn and Ni [61] found low P_n velocity of about 7.8 km/s beneath the Anatolian plate. Rodgers et al. [62] detected an inefficient S_n propagation, low P_n velocity, and volcanism indicating possible partial melt in the upper mantle beneath Turkey. Saunders et al. [63] detected a possible low-velocity zone in the upper mantle beneath station ANTO in central Turkey. Moreover, central Turkey is underlain by smaller scale (~ 200 km) very low (< 7.8 km/s) P_n velocity zones [64], which are interpreted to be regions of no mantle lid. Other similar studies in the Anatolian plate estimated the S_n velocity at around 4.3–4.5 km/s [65]. Recently, Erduran et al. [66] detected a shallow low shear wave velocity of 2.2 km/s that increases to 3.6 km/s at a depth of 10 km beneath Anatolia. The mid-crustal depth range is dominated by a weakly developed low-velocity zone having a shear wave velocity of 3.55 km/s. Moreover, they came to the conclusion that the estimated velocities are considerably lower than indicated by PREM in almost all depth ranges. The uppermost mantle beneath the Anatolian plate is represented by a relatively low shear wave velocity of 4.27 km/s. This observation is consistent with other similar results [67–70]. Anomalously low shear wave velocities were found by Gök et al. [71] underneath the Anatolian block and the Anatolian plateau in eastern Turkey. These low-velocity anomalies are probably related to the absence of

a lithospheric mantle lid and its replacement with asthenospheric materials. Laboratory experiments of mechanical behavior in mantle rocks, on the other hand, show that a V_s reduction as high as 7.9% can occur if the upper mantle contains 1% melt [72]. Inversion results of Tezel et al. [65] indicate that the Anatolian region has a low shear wave velocity zone at 7–20 km depths, and that shear wave velocities are faster beneath eastern Turkey than western Turkey. The low crustal velocities may be associated with high crustal temperatures, a high degree of fracture or the presence of fluids at high pore pressure in the crust [73]. In general, both the crustal and upper mantle shear velocities obtained for Turkey are lower than those obtained throughout most of Europe [65].

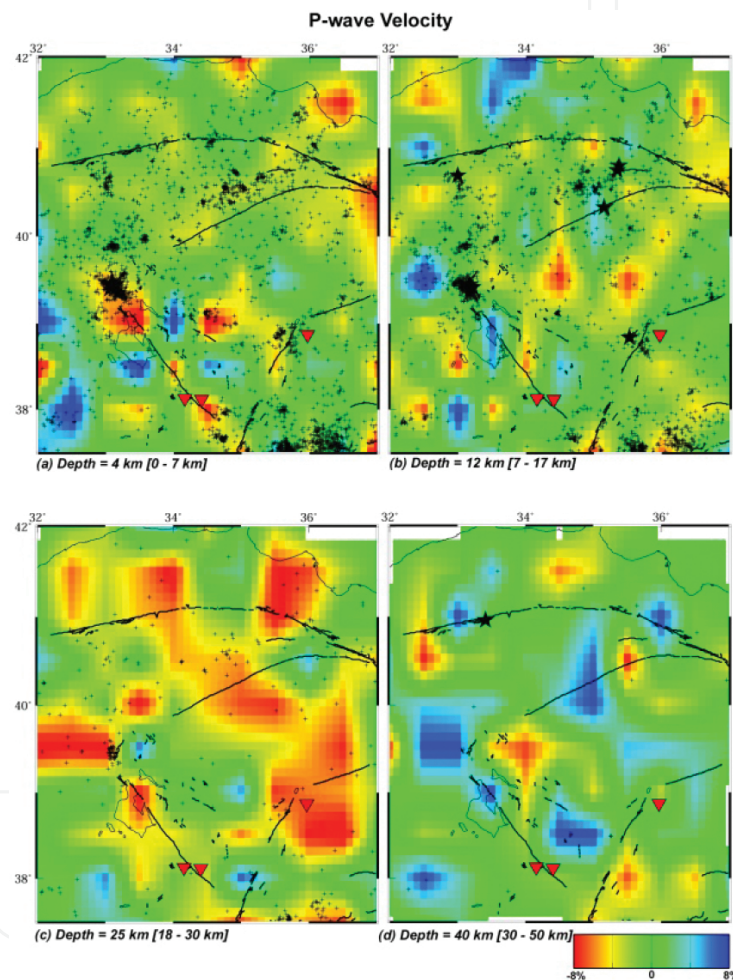


Figure 7. Compressional wave velocity structures (in percentages) at four depth slices: 4 (a), 12 (b), 25 (c), and 40 (d) km beneath central Anatolia. The low- and high-velocities are represented, respectively, by red and blue colors. The depth range of the microseismic activity, plotted as crosses, is given between brackets. Black stars denote the moderate and large earthquakes ($M \geq 5.0$) in the same depth range of the background seismicity. Active faults in central Anatolia are represented by the thin solid lines. Inverted red triangles denote Cenozoic volcanoes. The perturbation scale ($\pm 8\%$) is shown to the lower right.

Zor et al. [74] determined moderate to high L_g -attenuation values ($Q_0 \sim 100\text{--}200$) beneath the Turkish plateau, which probably originate from both scattering and intrinsic attenuation due

to the tectonic complexity and the wide-spread young volcanics in the region. It was found that the b -value shows different distributions along Turkey. Specifically, the central Anatolian plate has higher b -values than the average [75]. Koulakov et al. [76] detected low-velocity and high-attenuation anomalies, which are associated with both the fracturing zones of the western segment of the NAFZ and the sedimentary basins in western Anatolia. A Curie-point-depth (CPD) map for the Galatia Volcanic volcanic Complex in north central Turkey constructed by Bilim [58] shows high geothermal potential. The CPDs vary from about 6.74 to 16.9 km and are consistent with the results of previous geothermal studies. The complex exhibits low CPD and high heat flow values (>100 mW/m²). These high heat flow values, which are 60% above the world average, are consistent with the earlier results of Pollack et al. [77] and Ilkisik [78]. Moreover, the Bouguer anomaly map displays negative contour closure that may be related to the low-density distribution in the study area.

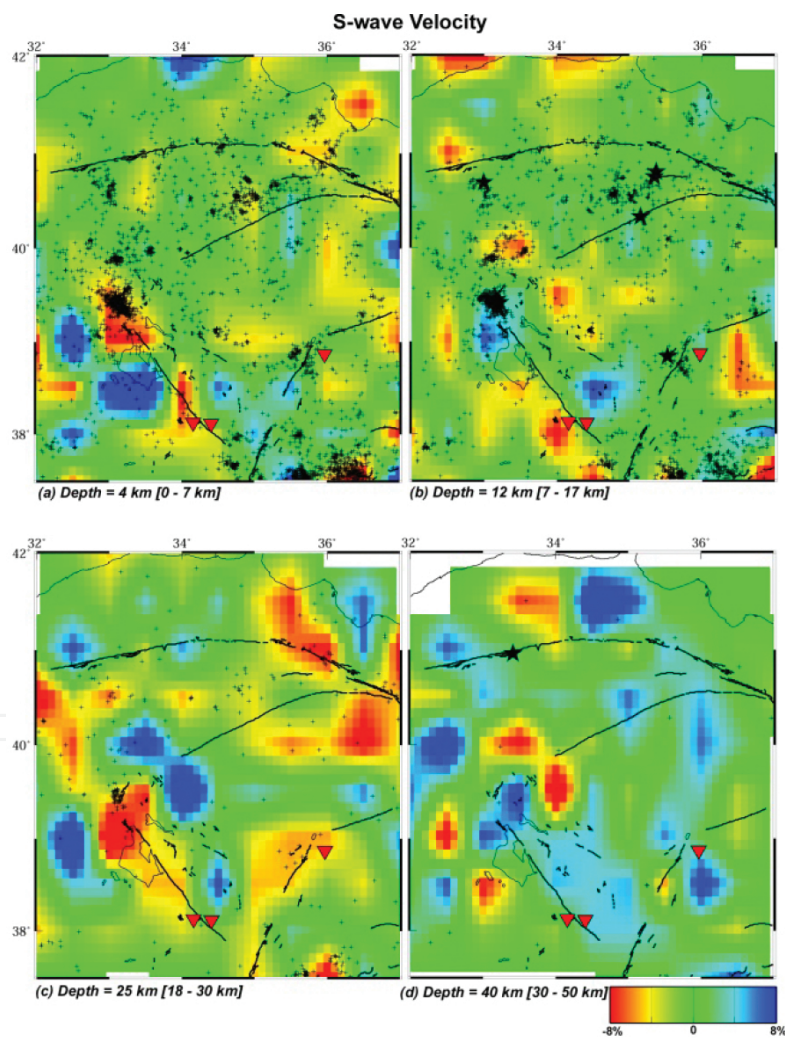


Figure 8. S-wave velocity structures at the four depth slices. Other details are similar to those of **Figure 7**.

In brief, central Anatolia is characterized by the presence of many sedimentary basins, extensive faulting, and Cenozoic volcanics. The mapped low-velocity/high V_p/V_s zones are

thus consistent with such circumstances. Moreover, many previous geophysical observations such as low P_n and S_n velocities, high S_n attenuation, high heat flow, shallow magnetic thickness, low L_g Q_0 -values, and high geothermal potential support the imaged low-velocity/high Vp/Vs ratio zones. The results of these geophysical observations beneath central Anatolia are similar to those detected beneath the Tibet and denote the existence of a partially molten, serpentinized mantle. This partial melt in the uppermost mantle represents the source of the widespread Cenozoic volcanism in the region.

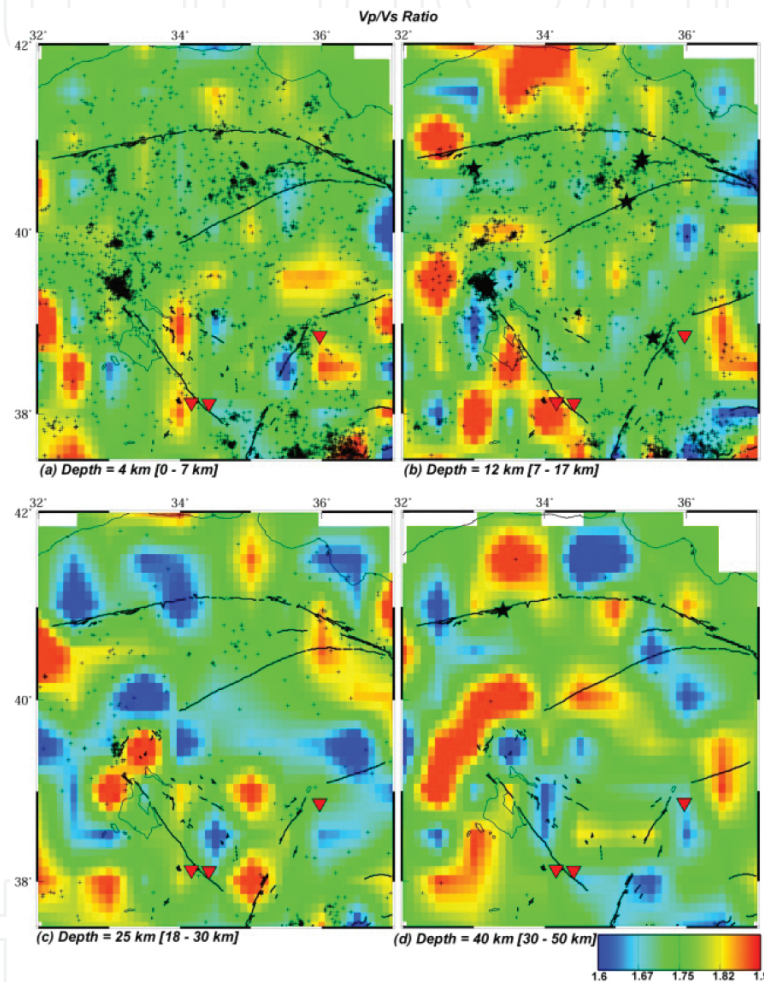


Figure 9. Distribution of Vp/Vs structures at four depth slices. Red and blue colors denote high and low Vp/Vs ratio, respectively. The variation scale (1.6–1.9) is shown to the lower right. Other details are similar to those of **Figure 7**.

5. 3D upper crustal structure north of the convergent boundary between the Eurasian and African plates

The 3D P - and S -wave velocity models of the upper crust beneath southwest (SW) Iberia in the western Mediterranean region is determined by inverting arrival time data from local earth-

quakes. The western Mediterranean region, including Iberia and northwest Africa, displays a variety of seismotectonic activities due to the interaction between the African and Eurasian plates [9, 79]. Active deformation in the Africa-Eurasia plate boundary zone is generally interpreted as the result of the oblique convergence between the African and Eurasian plates, ranging from ~ 10 mm/yr at the longitude of Turkey to ~ 4 mm/yr in the Gibraltar Strait according to the NUVEL1A global plate kinematic model [80, 81]. Between 14°W and the Gibraltar Strait, the plate boundary is not clearly defined and the convergence between Africa and Europe is accommodated through a broad, tectonically-active, deformation zone [82], where a considerable and diffuse seismic activity has long been recognized [83–87].

The geological evolution of SW Iberia during the Cenozoic is controlled mainly by the Alpine tectonic phases affecting most of southern Europe [88]. A large area of the central and western Iberian Peninsula is covered by the Variscan Iberian Massif, a large, old, and geologically stable block of continental lithosphere [89].

The margin of SW Iberia and the Afro-Eurasian convergence zone form an area of moderate to high seismicity, with sometimes earthquakes of $M \geq 5.0$, and are considered as being under the potential threat of natural hazards linked to seismicity and tsunami generation [91, 92]. Earthquakes are concentrated along regional-scale WSW–ENE lineaments in northern Algeria and easternmost Atlantic Ocean (**Figure 10**), presumably marking two segments of the convergent Africa–Eurasia plate boundary [90, 93]. In between, at the contact of Morocco and Spain, seismicity is distributed over a more than 400 km wide zone, and is characterized by lower magnitudes (usually < 5.5), compared to the adjacent sections [87]. These characteristics suggest a diffuse partitioning of plate convergence strain and complicate the definition of a plate boundary between Morocco and Spain. The seismic activity is generally shallow with most earthquakes having a focal depth < 20 km (**Figure 10**), and the lower crust is essentially aseismic. Relatively deep earthquakes occur in the off-shore along the southern and western borders of SW Iberia. The shallow cut-off depth of seismicity [94] and the short epicentral distances hinders the accurate imaging of the velocity structure of the lower crust in this region. Focal mechanisms of earthquakes along this segment of the plate boundary indicate thrust faulting in nearly E–W trending planes, with sometimes considerable strike-slip component. The deformation is expressed as compression at $N139^\circ$ at a rate of 4.5 mm/yr. The small component of extension (1.4 mm/yr) is the result of the strike-slip motion observed in some events [95]. Many authors assumed that regional $M \sim 6$ –7 earthquakes are generated by the Lower Tagus Valley fault in the westernmost part of SW Iberia around Lisbon City [96]. In addition, results of Montilla et al. [97] reveal that there are some Portuguese cities, like Lisbon and Coimbra, where the seismic hazard is entirely or almost entirely caused by local seismicity. They have also found that there are cities along the southern coast where seismic foci at 200 km away or more can be the most important or at least contribute significantly to the hazard such as Beja and Faro in Portugal and Cádiz and Huelva in Spain.

In this study, we use the available arrival time data to compute *P*- and *S*-wave velocity (as well as their ratio) models for the upper crust beneath SW Iberia and correlate them with the tectonics of the region and the previous geological and geophysical investigations.

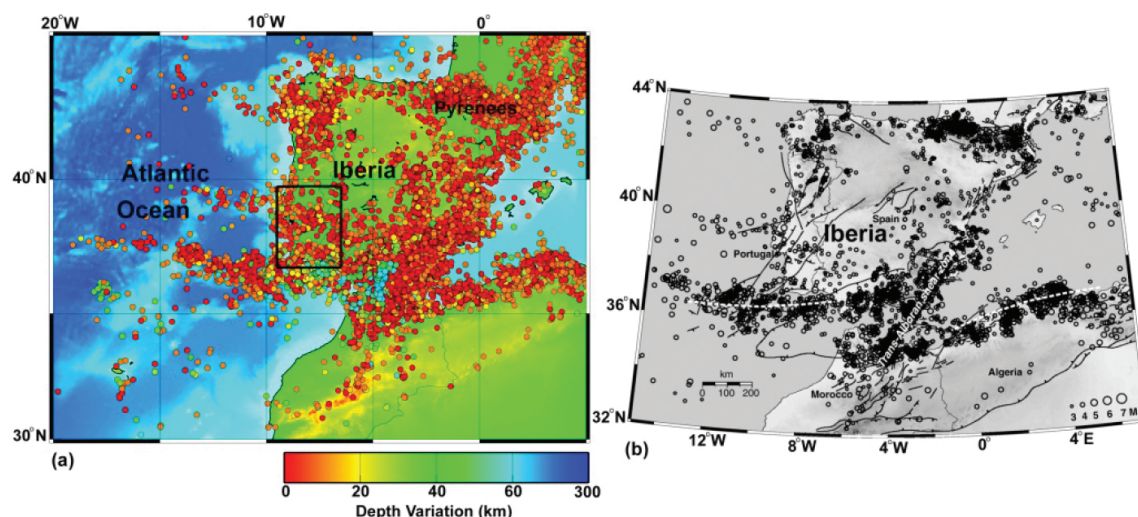


Figure 10. (a) Epicentral distribution of NEIC (US Geological Survey: <http://neic.usgs.gov>) seismicity in the western Mediterranean region. (b) Seismicity of the Ibero–Maghrebian region projected on the map of active and potentially active faults [90]. Epicenters of earthquake with local magnitude ≥ 3 (scale on lower right) are taken from the NEIC catalogue. Neotectonic faults (grey) are redrawn from the Geodynamic map of the Mediterranean compiled in the frame of the Commission for the Geological Map of the World (<http://ccgm.free.fr>).

5.1. Data

We used arrival time data of P - and S -waves from local earthquakes beneath SW Iberia. A total of 886 events occurring between latitudes 36.75 – 39.75°N and longitudes 6.5 – 9.5°W (**Figure 11**), from 2003 to 2007 are carefully selected from the preliminary seismological bulletins published by the Meteorological Institute (IM) of Portugal, which are available on the web (<http://www.meteo.pt>). The selected events are recorded by 21 seismic stations (**Figure 11**) belonging to the permanent seismic network operated by the IM of Portugal. Although the coverage of this network is good along the southern and western regions, few stations are available in the north and northwest with additionally low seismic activity. The method of Lienert and Havskov [98] is used for hypocenter location. These earthquakes were selected on the basis of minimum number of P - and S -wave recordings of at least 5, and the fact they have a uniform spatial distribution in the study area. Errors in the hypocentral locations do not exceed 10 km in horizontal directions, and 2–3 km in depth direction. Most land earthquakes are shallower than 20 km, while deep events (up to 45 km depth) occur in the south and southwest (**Figure 11**). The total numbers of P - and S -wave data are 3085, and 2780 arrivals, respectively. The accuracy of time picking is estimated to be ± 0.15 s; although may be larger up to ± 0.25 s, for less impulsive arrivals [see 93 for more details].

5.2. Results

Inversion results of V_p , V_s , and V_p/V_s distributions at two crustal layers are shown in **Figure 12**. Significant lateral variations of up to $\pm 6\%$ of velocity (V_p and V_s) and ± 0.2 of V_p/V_s ratio are revealed in the study area. Higher-than average P -wave velocity anomalies are revealed at 4 km depth, which change to low velocity at 12 km depth (**Figure 12a** and **b**). Although of smaller amplitudes relative the P -wave velocity anomalies, the S -wave velocity is generally higher than

the average at the two upper crustal layers with some patches of low S -wave velocity (**Figure 12c** and **d**). The V_p/V_s ratio is generally higher than the average except at some parts in the south at a depth of 12 km (**Figures 12e** and **f**). The high velocity and high V_p/V_s ratio zones are generally characterized by intense seismicity. The implications of the imaged velocity and V_p/V_s anomalies and their relation to other geophysical studies beneath SW Iberia are discussed briefly in the following paragraphs.

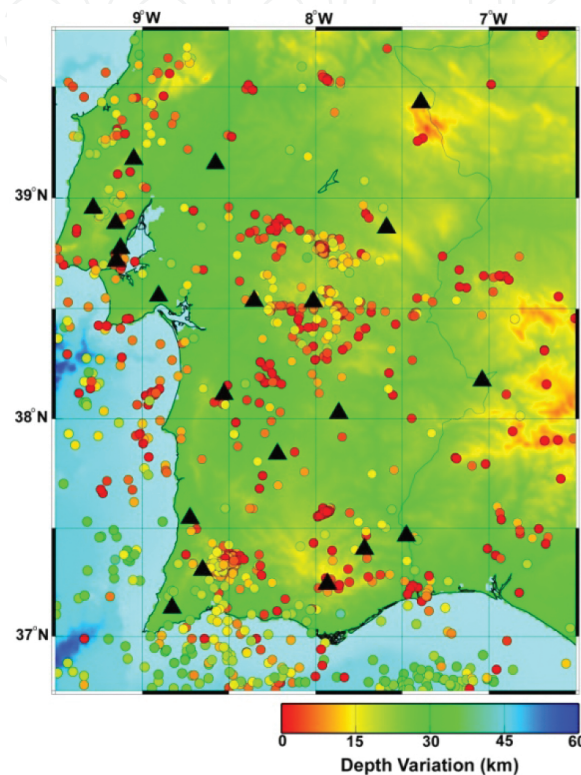


Figure 11. Epicentral distribution of the 886 earthquakes used in this study shown as circles, which vary in color according to the depth of the hypocenter (scale is at the bottom). The black triangles show the 21 seismic stations in SW Iberia used to record the selected events.

5.3. Discussion

5.3.1. Crustal velocity structure beneath SW Iberia

The shallow velocity structure of SW Iberia is generally characterized by higher than average velocity, which decreases clearly downward at a depth of 12 km especially for P -wave velocity. These shallow, high P - and S -wave velocities are consistent with the high P -wave velocities at depths of 7–10 km detected by González-Fernández et al. [99] and could be related to the mafic and ultramafic rocks in southern Portugal. Results of da Silva et al. [100] point to the existence of shallow resistive domains, which are consistent with the lithological and structural features observed and mapped in the region. The roots of the Beja Acebuches Ophiolite Complex are inferred from 12 km onwards, forming a moderate resistive band located between two middle-

crustal conductive layers. These conductive layers overlap the Iberian Reflective body and are interpreted as part of an important middle-crustal décollement developed immediately above or coinciding with the top of a graphite-bearing granulitic basement [100]. The heterogeneous velocity structure of the SW Iberian upper crust is consistent with the results of the mineralogical and petrological investigations carried out by Sánchez-Gracia et al. [101].

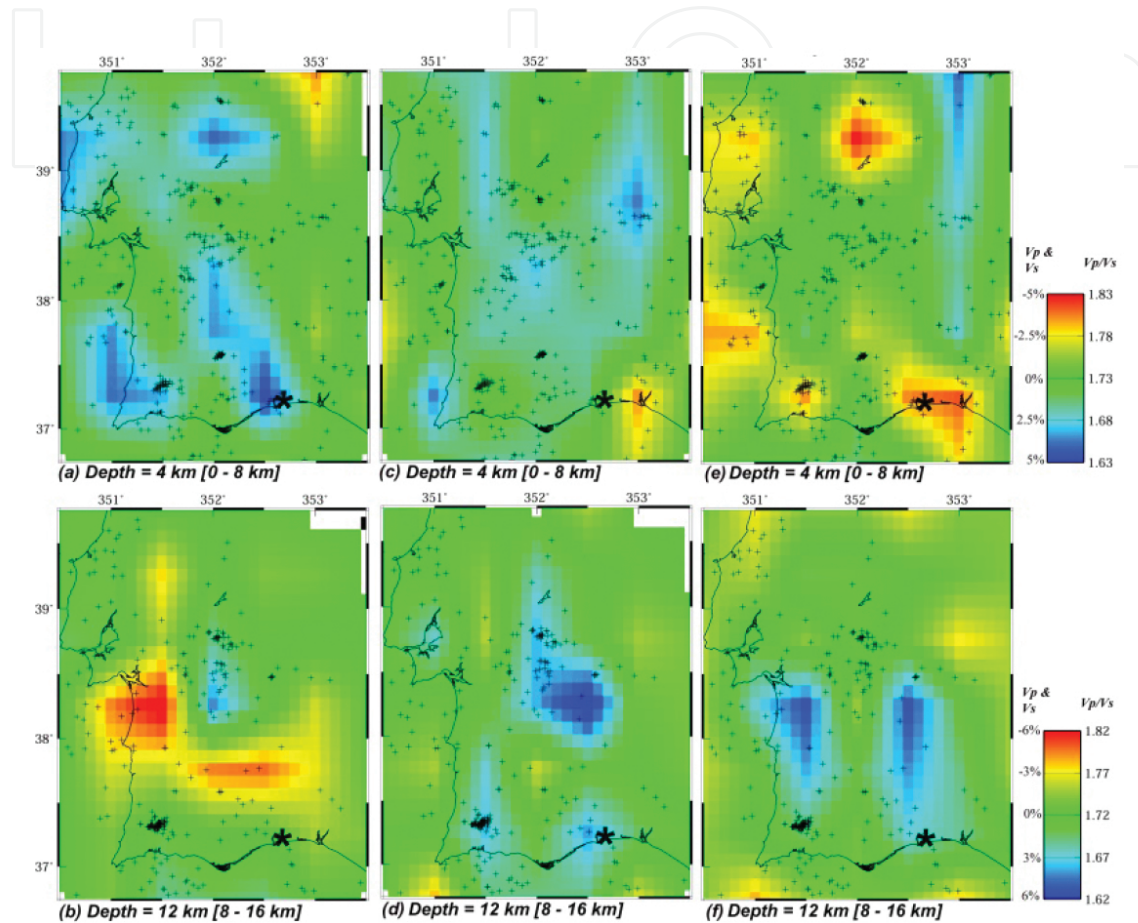


Figure 12. P -wave velocity [(a) and (b)], S -wave velocity [(c) and (d)], and V_p/V_s [(e) and (f)] crustal structures beneath SW Iberia at depths of 4 and 12 km. Low velocity and high V_p/V_s are indicated by red colors, whereas the blue colors denote high velocities and low V_p/V_s . Numbers between brackets show the depth range of the microseismic activity plotted as crosses. Black star denotes the 12 December, 1989 M 5.2 earthquake (focal depth = 14 km). The perturbation scales of velocity and V_p/V_s ratio at the two crustal depths are shown to the right.

Sánchez-Gracia et al. [102] noticed a pronounced increase of the geothermal gradient, which is indicated by partial melting of the metasedimentary protoliths in the upper and middle crust, and by coeval core-complex formation. These observations are consistent with the low-velocity and high V_p/V_s ratios, which are detected in the present study. The westernmost part of the study region, known as the Lower Tagus Valley, has many active or potentially-active faults [103], which are poorly understood because of thick sedimentary cover. However, reprocessing of seismic reflection profiles, aeromagnetic and seismicity data by Carvalho et al. [104], to locate and characterize the Ota-Vila Franca de Xira-Lisbon Sesimbra fault zone in the in SW Iberia, indicates that this fault could be a possible source of the $M_w = 6.0$ 1909 Benavente damaging

earthquake [105]. This region is characterized by low P -wave velocity, average S -wave velocities, and average to high V_p/V_s ratio (**Figure 12**), indicating possible fluid inclusions along the hidden fault zones, which may act as a trigger to the large damaging earthquakes.

5.3.2. Crustal V_p/V_s ratio beneath SW Iberia

It is thought that the average composition of the continental crust is close to andesite or diorite [106]. Laboratory measurements of the V_p/V_s ratio of diorite at crustal pressures are in the range of 1.75–1.79 [107]. SW Iberia exhibits high crustal V_p/V_s ratios that might be caused by the inclusion of partial melt and/or fluids in such a tectonically active region. Results of receiver function analysis beneath the Lower Tagus Valley along the western coast of the present study region by Salah et al. [108] confirm this tectonic activity, where it reveals a thinner-than-expected crust that is characterized by high V_p/V_s ratios. In these areas, fluids released from the dehydration reactions in subducting slabs or ascending out along fractures and faults following spreading and rifting processes penetrate the overlying crustal rocks and increase the crustal V_p/V_s ratio [109, 110]. The results of the 2-D inversion of magnetotelluric data set by Santos et al. [111] and Pous et al. [112] in SW Iberia revealed high conductivity layers coinciding with the transitions among different suture zones and were interpreted as related to fluids along faults. These conductive bodies related to sutures at depth (sometimes as deep as 15–25 km) were caused by graphite enrichments carried by fluids passing along shear zones formed due to the overall transpressive regime. It was also found that the top part of some of these conductive layers correlates spatially with a broad reflector detected by a recently acquired deep seismic reflection profile whose origin has been interpreted as a mafic intrusion [113]. High mean heat flow (~ 100 mW/m²) was observed by Duque and Mendes-Victor [114], and at some sites they even reported values above 100 mW/m², which was unexpected for regions like SW Iberia. Moreover, the intensive faulting detected in large areas in SW Iberia might serve as passage ways for ascending fluids from the uppermost mantle and can explain the high crustal V_p/V_s ratios. However, more information about the crustal V_p/V_s variations at much deeper layers from higher quality and larger quantity of seismological data is necessary to reach robust conclusions and interpretations.

6. Conclusions

From the results obtained for the two studied areas, we can outline the following points:

1. The crustal velocity structure beneath central Anatolia is characterized generally by lower-than-average velocity. The low-velocity zones are more prominent beneath the active fault segments and the volcanic provinces.
2. High V_p/V_s ratio zones are clearly visible at almost all depth slices, which are consistent with the possibility of the existence of partial melt in the lower crust and the uppermost mantle beneath central Anatolia.

3. Although some events occur in high-velocity zones; most of the large and small earthquakes are closely associated with low-velocity/high V_p/V_s ratio zones and are intense near active faults and heterogeneous zones in the study region.
4. The shallow velocity structure beneath SW Iberia is dominated by higher-than-average seismic wave velocities, which change downward to lower velocity especially along the coastal areas and are related to the mafic and ultramafic rocks in south Portugal.
5. High V_p/V_s zones are clearly visible at the two upper crustal layers especially along the coast of the Atlantic Ocean that are consistent with the possibility of the existence of fluids in the crust. The latter is evidenced by the presence of conductive and reflector bodies in the upper-middle crust beneath large portions of SW Iberia.
6. The mapped velocity V_p/V_s zones in the upper crust of SW Iberia are consistent with many geophysical evidences such as high heat flow, the presence of some conductive layers at depth, intensive faulting, and shearing, as well as the presence of some reflectors that are detected by seismic reflection surveying.

Author details

Mohamed K. Salah

Address all correspondence to: ms264@aub.edu.lb

Department of Geology, American University of Beirut, Beirut, Lebanon

References

- [1] Zhao D. New advances of seismic tomography and its applications to subduction zones and earthquake fault zones: a review. *The Island Arc*. 2001;10:68–84.
- [2] Zhao D, Negishi H. The 1995 Kobe earthquake: seismic image of the source zone and its implications for the rupture nucleation. *J. Geophys. Res.* 1998;103:9967–9986.
- [3] Allam AA, Ben-Zion Y. Seismic velocity structures in the southern California plate-boundary environment from double-difference tomography. *Geophys. J. Int.* 2012;190. DOI: 10.1111/j.1365-246X.2012.05544.x
- [4] Allam AA, Ben-Zion Y, Kurzon I, Vernon F. Seismic velocity structure in the hot springs and trifurcation areas of the San Jacinto fault zone, California, from double-difference tomography. *Geophys. J. Int.* 2014;198:978–999. DOI: 10.1093/gji/ggu176
- [5] Yeats RS, Sieh K, Allen CR. *The geology of earthquakes*. Oxford University Press Inc.; New York 1997. 568 p.

- [6] Yang H. Recent advances in imaging crustal fault zones: a review. *Earthq. Sci.* 2015;28(2):151–162. DOI: 10.1007/s11589-015-0114-3
- [7] Hasegawa A, Nakajima J, Umino N, Miura S. Deep structure of the northeastern Japan arc and its implications for crustal deformation and shallow seismic activity. *Tectonophysics.* 2005;403:59–75. DOI: 10.1016/j.tecto.2005.03.018
- [8] Christensen NI. In: James DE. (Ed.). *The Encyclopedia of Solid Earth Geophysics.* Springer-Verlag US 1989; ISBN 0-442-24366-9.
- [9] Serrano I, Zhao D, Morales J. 3-D crustal structure of the extensional Granada Basin in the convergent boundary between the Eurasian and African plates. *Tectonophysics.* 2002;344:61–79.
- [10] Sanders CO, Ponko SC, Nixon LD, Schwartz EA. Seismological evidence for magmatic and hydrothermal structure in Long Valley Caldera from local earthquake attenuation and velocity tomography. *J. Geophys. Res.* 1995;100:8311–8326. DOI: 10.1029/95JB00152
- [11] Wu H, Lees JM. Three-dimensional *P* and *S* wave velocity structures of the Coso Geothermal Area, California, from microseismic travel time data. *J. Geophys. Res.* 1999;104. DOI: 10.1029/1998JB900101
- [12] Lees JM, Wu H. Poisson's ratio and porosity at Coso geothermal area, California. *J. Volcanol. Geotherm. Res.* 2000;95:157–173.
- [13] Iverson WP, Fahmy BA, Smithson SB. *V_p/V_s* from mode converted P-SV reflections. *Geophysics.* 1989;54:843–852.
- [14] Tatham RH. *V_p/V_s* and lithology. *Geophysics.* 1982;47:336–344.
- [15] Holbrook WS, Gajewski P, Kramer A, Prodehl C. An interpretation of wide-angle compressional and shear wave data in southwest Germany: Poisson's ratio and petrological implications. *J. Geophys. Res.* 1988;93:12081–12106.
- [16] Zhao D, Hasegawa A, Horiuchi S. Tomographic imaging of *P* and *S* wave velocity structure beneath northeastern Japan. *J. Geophys. Res.* 1992;97:19909–19928.
- [17] Zhao D, Hasegawa A, Kanamori H. Deep structure of Japan subduction zones as derived from local, regional and teleseismic events. *J. Geophys. Res.* 1994;99:22313–22329.
- [18] Zhao D, Yanada T, Hasegawa A, Umino N, Wei W. Imaging the subducting slabs and mantle upwelling under the Japan Islands. *Geophys. J. Int.* 2012;190:816–828.
- [19] Um J, Thurber C. A fast algorithm for two-point seismic ray tracing. *Bull. Seismol. Soc. Am.* 1987;77:972–986.
- [20] Christensen NI. Poisson's ratio and crustal seismology. *J. Geophys. Res.* 1996;101:3139–3156.

- [21] Zhao D, Tani H, Mishra OP. Crustal heterogeneity in the 2000 western Tottori earthquake region: effect of fluids from slab dehydration. *Phys. Earth Planet. Inter.* 2004;145:161–177.
- [22] Baris S, Nakajima J, Hasegawa A, Honkura Y, Ito A, Üçer SB. Three-dimensional structure of V_p , V_s , and V_p/V_s in the upper crust of the Marmara region, NW Turkey. *Earth Planets Space.* 2005;57:1019–1038.
- [23] Salah MK, Sahin S, Destici C. Seismic velocity and Poisson's ratio tomography of the crust beneath southwest Anatolia: an insight into the occurrence of large earthquakes. *J. Seismol.* 2007;11:415–432. DOI: 10.1007/s10950-007-9062-2
- [24] Salah MK, Sahin S, Aydin U. Seismic velocity and Poisson's ratio tomography of the crust beneath east Anatolia. *J. Asian Earth Sci.* 2011;40:746–761.
- [25] Janik T. Upper lithospheric structure in the central Fennoscandian Shield: constraints from P- and S-wave velocity models and V_p/V_s ratio distribution of the BALTIC wide-angle seismic profile. *Acta Geophys.* 2010;58(4):543–586. DOI: 10.2478/s11600-010-0002-0
- [26] Kayal JR, Zhao D, Mishra OP, De R, Singh OP. The 2001 Bhuj earthquake: tomographic evidence for fluids at the hypocenter and its implications for rupture nucleation. *Geophys. Res. Lett.* 2002;29(24): 2152. DOI: 10.1029/2002GL015177
- [27] Zhao D, Mishra OP, Sanda R. Influence of fluids and magma on earthquakes: seismological evidence. *Phys. Earth Planet. Inter.* 2002;132:249–267.
- [28] Salah MK, Zhao D. 3-D seismic structure of Kii Peninsula in southwest Japan: evidence for slab dehydration in the forearc. *Tectonophysics.* 2003;364:191–213. DOI: 10.1016/S0040-1951(03)00059-3
- [29] Salah MK, Sahin S, Topatan U. Crustal velocity and V_p/V_s structures beneath central Anatolia from local seismic tomography. *Arab. J. Geosci.* 2014;7:4101–4118. DOI 10.1007/s12517-013-1038-7
- [30] McClusky S, Balassanian S, Barka A, Demir C, Ergintav S, Georgiev I, Gurkan O, Hamburger M, Hurst K, Kahle H, Kastens K, Kekelidze G, King R, Kotzev V, Lenk O, Mahmoud S, Mishin A, Nadariya M, Ouzounis A, Paradissis D, Peter Y, Prilepin M, Reilinger R, Sanli I, Seeger H, Tealeb A, Toksöz MN, Veis G. Global positioning system constrains on plate kinematics and dynamics in the eastern Mediterranean and Caucasus. *J. Geophys. Res.* 2000;105:5695–5719.
- [31] Hubert-Ferrari A, King G, Manighetti I, Armijo R, Meyer B, Tapponnier P. Long-term elasticity in the continental lithosphere; modeling the Aden Ridge propagation and the Anatolian extrusion process. *Geophys. J. Int.* 2003;153:111–132.
- [32] Eaton S, Robertson AHF. The Miocene Pakhour Formation, southern Cyprus, and its relation to the Neogene tectonic evolution of the eastern Mediterranean. *Sediment. Geol.* 1993;86:273–292.

- [33] Sengör AMC. Mid-Mesozoic closure of Permo-Triassic Tethys and its implications. *Nature*. 1979;279:590–593.
- [34] Rotstein Y. Counterclockwise rotation of Anatolian block. *Tectonophysics*. 1984;108:71–91.
- [35] Sengör AMC, Görür N, Saroğlu F. Strike-slip faulting and related basin formation in zones of tectonic escape: Turkey as a case study, in: Biddle KT, Christie-Blick N. (Eds.), *Strike-slip Faulting and Basin Formation*. Soc. Econ. Paleontol. Mineral. Spec. Pub. 1985;37:227–264.
- [36] Tatar O, Piper JDA, Park RG, Gürsoy H. Palaeomagnetic study of block rotations in the Niksar overlap region of the North Anatolian Fault Zone, central Turkey. *Tectonophysics*. 1995;244:251–266.
- [37] Bozkurt E, Koçyiğit A. The Carova basin: an active negative flower structure on the Almus fault zone, a splay fault system of the North Anatolian Fault Zone. *Tectonophysics*. 1996;265:239–254.
- [38] Barka AA, Reilinger R. Active tectonics of the eastern Mediterranean region deduced from GPS, neotectonic, and seismicity data. *Ann. Geofis.* 1997;40:587–610.
- [39] Reilinger RE, McClusky SC, Oral MB, King W, Toksöz MN. Global positioning system measurements of present-day crustal movements in the Arabian–Africa–Eurasia plate collision zone. *J. Geophys. Res.* 1997;102:9983–9999.
- [40] Ketin İ. Relations between general tectonic features and the main earthquake regions of Turkey. *Min. Res. Explor. Inst. Bull.* 1968;71:63–67.
- [41] Kiratzi AA. A study of the active crustal deformation of the North and East Anatolian fault zones. *Tectonophysics*. 1993;225:191–203.
- [42] Cianetti S, Gasperini P, Giunchi C, Boschi E. Numerical modeling of the Aegean-Anatolian region: geodynamical constraints from observed rheological heterogeneities. *Geophys. J. Int.* 2001;146:760–780.
- [43] Faccenna C, Bellier O, Martinod J, Piromallo C, Regard V. Slab detachment beneath eastern Anatolia: a possible cause for the formation of the North Anatolian Fault. *Earth Planet Sci. Lett.* 2006;242:85–97.
- [44] Le Pennec JL, Bourdier JL, Froger JL, Temel A, Camus G, Gourgaud A. Neogene ignimbrite of the Nevşehir Plateau (central Turkey): stratigraphy, distribution and source constraints. *J. Volcanol. Geotherm. Res.* 1994;63:59–87.
- [45] Aydar E, Gourgaud A, Deniel C, Lyberis N, Gundogdu N. Le volcanisme quaternaire d'Anatolie centrale (Turquie): association de magmatisme calco-alcalin et alcalin en domaine de convergence. *Can. J. Earth Sci.* 1995;32:1058–1069.
- [46] Barka AA. The North Anatolian Fault zone. *Ann. Tecton.* 1992;6:164–195.

- [47] Westaway R. Present-day kinematics of the Middle East and Eastern Mediterranean. *J. Geophys. Res.* 1994;99:12071–12090.
- [48] Taymaz T, Jackson J, McKenzie D. Active tectonics of the north and central Aegean Sea. *Geophys. J. Int.* 1991;108:422–490.
- [49] Oral MB, Reilinger RE, Toksöz MN, Kong RW, Barka AA, Kınık İ, Lenk O. Global positioning system offers evidence of plate motions in eastern Mediterranean. *EOS Transac.* 1995; 76 (9).
- [50] Armijo R, Meyer B, Barka AA, Hubert A. Propagation of the North Anatolian Fault into the Northern Aegean: timing and kinematics. *Geology.* 1999;27:267–270.
- [51] Barka AA, Akyüz SH, Cohen HA, Watchorn F. Tectonic evolution of the Nıksar and Tasova-Erbaa pull-apart basins, North Anatolian Fault Zone: their significance for the motion of the Anatolian block. *Tectonophysics.* 2000;322:243–264.
- [52] Bozkurt E. Neotectonics of Turkey—a synthesis. *Geodin. Acta.* 2001;14:3–30.
- [53] Koçyiğit A, Özacar AA. Extensional neotectonic regime through the NE edge of the Outer Isparta Angle, SW Turkey: new field and seismic data. *Turkish J. Earth Sci.* 2003;12:67–90.
- [54] Herrin E. Seismological tables for *P*-phases. *Bull. Seismol. Soc. Am.* 1968;60:461–489.
- [55] Lee WHK, Lahr JC. HYP071: a computer program for determining hypocenter, magnitude, and first motion pattern of local earthquakes. Open File Report, U. S. Geological Survey, 1972; 100 p.
- [56] Saroğlu F, Emre Ö, Kusçu İ. Map of Active Faults in Turkey. General Directorate of Turkish Mineral Research and Exploration Institute, Ankara, Turkey; 1992.
- [57] Sengör AMC, Yılmaz Y. Tethyan evolution of Turkey: a plate tectonic approach. *Tectonophysics.* 1981;75:181–241.
- [58] Bilim F. Investigation of the Galatian volcanic complex in the northern central Turkey using potential field data. *Phys. Earth Planet Inter.* 2011;185:36–43. DOI:10.1016/j.pepi.2011.01.001
- [59] Jaffey N, Robertson A, Pringle M. Latest Miocene and Pleistocene ages of faulting, determined by $^{40}\text{Ar}/^{39}\text{Ar}$ single-crystal dating of air-fall tuff and silicic extrusives of the Erciyes Basin, central Turkey: evidence for intraplate deformation related to the tectonic escape of Anatolia. *Terra Nova.* 2004;16:45–53. DOI: 10.1111/j.13653121.2003.00526.x
- [60] Gürbüz C, Evans JR. A seismic refraction study of the western Tuzgölü basin, central Turkey. *Geophys. J. Int.* 1991;106:239–251.
- [61] Hearn TM, Ni JF. *P_n* velocities beneath continental collision zones: the Turkish-Iranian Plateau. *Geophys. J. Int.* 1994;117:273–283.

- [62] Rodgers AJ, Ni JF, Hearn TM. Propagation characteristics of short-period S_n and L_g in the Middle East. *Bull. Seismol. Soc. Am.* 1997;87:396–413.
- [63] Saunders P, Priestley K, Taymaz T. Variations in the crustal structure beneath western Turkey. *Geophys. J. Int.* 1998;134:373–389.
- [64] Al-Lazki AI, Sandvol E, Seber D, Barazangi M, Turkelli N, Mohamad R. P_n tomographic imaging of mantle lid velocity and anisotropy at the junction of the Arabian, Eurasian and African plates. *Geophys. J. Int.* 2004;158:1024–1040. DOI: 10.1111/j.1365246X.2004.02355x
- [65] Tezel T, Erduran M, Alptekin Ö. Crustal shear wave velocity structure of Turkey by surface wave dispersion analysis. *Ann. Geophys.* 2007;50:177–190.
- [66] Erduran M, Çakir Ö, Tezel T, Sahin S, Alptekin Ö. Anatolian surface wave evaluated at GEOFON station ISP Isparta, Turkey. *Tectonophysics.* 2007;434:39–54.
- [67] Meier T, Dietrich K, Stöckhert B, Harjes HP. One-dimensional models of shear wave velocity for the eastern Mediterranean obtained from the inversion of Rayleigh wave phase velocities and tectonic implications. *Geophys. J. Int.* 2004;156:45–58.
- [68] Karagianni EE, Papazachos CB, Panagiotopoulos DG, Suhadolc P, Vuan A, Panza GF. Shear velocity structure in the Aegean area obtained by inversion of Rayleigh waves. *Geophys. J. Int.* 2005;160:127–143.
- [69] Pasyanos ME. A variable resolution surface wave dispersion study of Eurasia, North Africa, and surrounding regions. *J. Geophys. Res.* 2005;110:B12301. DOI: 10.1029/2005JB003749
- [70] Maggi A, Priestly K. Surface waveform tomography of the Turkish–Iranian plateau. *Geophys. J. Int.* 2005;160:1068–1080.
- [71] Gök R, Pasyanos ME, Zor E. Lithospheric structure of the continent–continent collision zone: eastern Turkey. *Geophys. J. Int.* 2007;169:1079–1088. DOI: 10.1111/j.1365-246X.2006.03288.x
- [72] Hammond CW, Humphreys ED. Upper mantle seismic wave velocity: effects of realistic partial melt geometries. *J. Geophys. Res.* 2000;105:10975–10986.
- [73] Akyol N, Zhu L, Mitchell BJ, Sözbilir H, Kekovalý K. Crustal structure and local seismicity in western Anatolia. *Geophys. J. Int.* 2006. DOI: 10.1111/j.1365246X.2006.03053
- [74] Zor E, Sandvol E, Xie J, Türkelli N, Mitchell B, Gasanov AH, Yetirmishli G. Crustal attenuation within the Turkish plateau and surrounding regions. *Bull. Seismol. Soc. Am.* 2007;97:151–161. DOI: 10.1785/0120050227
- [75] Kalyoncuoglu UY. Evaluation of seismicity and seismic hazard parameters in Turkey and surrounding area using a new approach to the Gutenberg-Richter relation. *J. Seismol.* 2007;11:131–148. DOI: 10.1007/s10950-006-9041-z

- [76] Koulakov I, Bindi D, Parolai S, Grosser H, Milkereit C. Distribution of seismic velocities and attenuation in the crust beneath the North Anatolian Fault (Turkey) from local earthquake tomography. *Bull. Seismol. Soc. Am.* 2010;100:207–224. DOI: 10.1785/0120090105
- [77] Pollack HM, Hurter SJ, Johnson JR. Heat flow from the Earth's interior: analysis of the global data set. *Rev. Geophys.* 1993;31:267–280.
- [78] Ilkisik OM. Regional heat flow in western Anatolia using silica temperature estimates from thermal springs. *Tectonophysics.* 1995;244:175–184.
- [79] Serpelloni E, Vannucci G, Pondrelli S, Argnani A, Casula G, Anzidei M, Baldi P, Gasperini P. Kinematics of the western Africa-Eurasia plate boundary from focal mechanisms and GPS data. *Geophys. J. Int.* 2007;169. DOI: 10.1111/j.1365246X.2007.03367.x
- [80] De Mets C, Gordon RG, Argus DF, Stein S. Current plate motions. *Geophys. J. Int.* 1990;28:2121–2124.
- [81] De Mets C, Gordon RG, Argus DF, Stein S. Effect of recent revisions to the geomagnetic reversal time scale on estimates of current plate motions. *Geophys. Res. Lett.* 1994;21:2191–2194.
- [82] Sartori R, Torelli L, Zitellini N, Peis D, Lodolo E. Eastern segment of the Azores-Gibraltar line (central-eastern Atlantic): an ocean plate boundary with diffuse compressional deformation. *Geology.* 1994;22:555–558.
- [83] Fukao Y. Thrust faulting at a lithospheric plate boundary: the Portugal earthquake of 1969. *Earth Planet Sci. Lett.* 1973;18:205–216.
- [84] Udías A, Arroyo AL, Mezcuca J. Seismotectonics of the Azores–Alboran region. *Tectonophysics.* 1976;31:269–289.
- [85] Grimison NL, Chen WP. The Azores–Gibraltar plate boundary: focal mechanisms, depths of the earthquakes, and their tectonic implication. *J. Geophys. Res.* 1986;91:2029–2047.
- [86] Buforn E, Udías A, Colombás MA. Seismicity, source mechanisms and tectonics of the Azores-Gibraltar plate boundary. *Tectonophysics.* 1988;152:89–118.
- [87] Buforn E, Sanz de Galdeano C, Udías A. Seismotectonics of the Ibero-Maghrebian region. *Tectonophysics.* 1995;248:247–261.
- [88] Maldonado A, Somoza L, Pallarés L. The Betic orogen and the Iberian-African boundary in the Gulf of Cadiz: geological evolution (central North Atlantic). *Mar. Geol.* 1999;155:9–43.
- [89] Dallmeyer RD, Martínez García E. (Eds.), *Pre-Mesozoic Geology of Iberia* (Springer-Verlag, Berlin, Heidelberg, New York, 1990), 416 p.

- [90] Stich D, Serpelloni E, Mancilla F, Morales J. Kinematics of the Iberia-Maghreb plate contact from seismic moment tensors and GPS observations. *Tectonophysics*. 2006;426:295–317.
- [91] Zitellini N, Rovere M, Terrinha P, Chierici F, Matias L, Victor LM, Corela C, Ribeiro A, Cordoba D, Danobeitia JJ, Grácia E, Bartolomé R, Nicolich R, Pellis G, Vedora BD, Sartori R, Torelli L, Correggiari A, Vigliotti L. Neogene through quaternary tectonic reactivation of SW Iberian passive margin. *Pure Appl. Geophys*. 2004;161:565–587.
- [92] Reicherter K, Hübscher C. Evidence for a seafloor rupture of the Carboneras Fault Zone (southern Spain): relation to the 1522 Almería earthquake? *J. Seismol*. 2007;11:15–26. DOI: 10.1007/s10950-006-9024-0
- [93] Salah MK. Upper crustal structure beneath Southwest Iberia north of the convergent boundary between the Eurasian and African plates. *Geosci. Front*. 2014;5:845–854. <http://dx.doi.org/10.1016/j.gsf.2013.10.002>
- [94] Morales J, Serrano I, Vidal F, Torcal F. The depth of the earthquake activity in the Central Betic (Southern Spain). *Geophys. Res. Lett*. 1997;24:3289–3292.
- [95] Kiratzi AA, Papazachos CB. Active crustal deformation from the Azores triple junction to the Middle East. *Tectonophysics*. 1995;243:1–24.
- [96] Cabral J, Moniz C, Ribeiro P, Terrinha P, Matias L. Analysis of seismic reflection data as a tool for the seismotectonic assessment of a low activity intraplate basin – the Lower Tagus Valley (Portugal). *J. Seismol*. 2003;7:431–447.
- [97] Montilla JAP, Casado CL, Romero JH. Deaggregation in magnitude, distance, and azimuth in the south and west of the Iberian Peninsula. *Bull. Seismol. Soc. Am*. 2002;92:2177–2185.
- [98] Lienert BR, Havskov J. A computer program for locating earthquakes both locally and globally. *Seismol. Res. Lett*. 1995;66:26–36. <http://dx.doi.org/10.1785/gssrl.66.5.26>
- [99] González-Fernández A, Córdoba D, Vegas R, Matias LM. Seismic crustal structure in the southwest of the Iberian Peninsula and the Gulf of Cadiz. *Tectonophysics*. 1998;296:317–331.
- [100] da Silva NV, Mateus A, Santos FAM, Almeida EP, Pous J. 3-D electromagnetic imaging of a Palaeozoic plate-tectonic boundary segment in SW Iberian Variscides (S Alentejo, Portugal). *Tectonophysics*. 2007;445:98–115.
- [101] Sánchez-Gracia T, Quesada C, Bellido F, Dunning GR, del Tánago JG. Two-step magma flooding of the upper crust during rifting: the early Paleozoic of the Ossa Morena Zone (SW Iberia). *Tectonophysics*. 2008;461:72–90.
- [102] Sánchez-Gracia T, Bellido F, Quesada C. Geodynamic setting and geochemical signatures of Cambrian-Ordovician rift-related igneous rocks (Ossa-Morena Zone, SW Iberia). *Tectonophysics*. 2003;365:233–255. DOI:10.1016/S0040-1951(03)00024-6

- [103] Vilanova SP, Nunes CF, Fonseca JFBD. Lisbon 1755: a case of triggered onshore rupture. *Bull. Seismol. Soc. Am.* 2003;93:2056–2068.
- [104] Carvalho J, Rabeh T, Cabral J, Carrilho F, Miranda JM. Geophysical characterization of the Ota-Vila Franca de Xira-Lisbon-Sesimbra fault zone, Portugal. *Geophys. J. Int.* 2008;174:567–584. DOI:10.1111/j.1365-246X.2008.03791.x
- [105] Stich D, Batlló J, Macià R, Teves-Costa P, Morales J. Moment tensor inversion with single-component historical seismograms: the 1909 Benavente (Portugal) and Lambesc (France) earthquakes. *Geophys. J. Int.* 2005;162:850–858. DOI:10.1111/j.1365-246X.2005.02680.x
- [106] Anderson DL. *Theory of the Earth*. Blackwell Sci., Malden, MA. 1989.
- [107] Carmichael RS. *Handbook of physical properties of rocks*. CRC Press, Boca Raton, FL. 1982.
- [108] Salah MK, Chang SJ, Fonseca JFBD. Crustal structure beneath the Lower Tagus Valley, southwestern Iberia using joint analysis of teleseismic receiver functions and surface wave dispersion. *Geophys. J. Int.* 2011; 184:919-933. DOI: 10.1111/j.1365-246X.2010.04891.x
- [109] Owens TJ, Zandt G. Implications of crustal property variations for models of Tibetan plateau evolution. *Nature*. 1997;387:37–43.
- [110] Nakajima J, Matsuzawa T, Hasegawa A, Zhao D. Three-dimensional structure of V_p , V_s , and V_p/V_s beneath northeastern Japan: implications for arc magmatism and fluids. *J. Geophys. Res.* 2001;106:21843–21857.
- [111] Santos FAM, Mateus A, Almeida EP, Pous J, Mendes-Victor LA. Are some of the deep crustal conductive features found in SW Iberia caused by graphite. *Earth Planet Sci. Lett.* 2002;201:353–367.
- [112] Pous J, Muñoz G, Heise W, Melgarejo CJ, Quesada C. Electromagnetic imaging of Variscan crustal structures in SW Iberia: the role of interconnected graphite. *Earth Planet Sci. Lett.* 2004;217:435–450. DOI: 10.1016/S0012-821X(03)00612-5
- [113] Simancas F, Carbonell R, Lodeiro FG, Estaún AP, Juhlin C, Ayarza P, Kashubin A, Azor A, Poyatos DM, Almodóvar GR, Pascual E, Sáez R, Expósito I. The crustal structure of the transpressional Variscan orogen of SW Iberia: The IBERSEIS deep seismic profile. *Tectonics*. 2003;22:1062.
- [114] Duque MR, Mendes-Victor LA. Heat flow and deep temperature in South Portugal. *Stud. Geophys. Geodyn.* 1993;37:279–292.